International Journal of Engineering Inventions
e-ISSN: 2278-7461, p-ISSN: 2319-6491
Volume 15, Issue 1 [January 2026] PP: 58-69

Robust H_∞ Control of A Synchronverter-Based LVDC Microgrid With Fault Ride-Through Capability

Miharisoa Faniry Rabarisoa Ririva, Apotheken Gericha Rabearivelo, Andry Auguste Randriamitansoa

Doctoral School in Engineering Sciences, Technology and Innovation, University of Antananarivo, Madagascar
Corresponding Author: Miharisoa Faniry Rabarisoa Ririva

ABSTRACT: *This paper investigates the modeling and control of a low-voltage DC (LVDC) microgrid interfaced with an AC macro-grid through a synchronverter operating in grid-forming mode. A detailed small-signal state-space model is developed including DC-bus dynamics, virtual frequency and active/reactive power states, with explicit representation of virtual inertia, damping and internal droop couplings. A multivariable robust H_∞ controller is designed on a reduced-order model using standard performance, control-effort and uncertainty weighting functions. The controller is evaluated against a classical droop PI benchmark under two representative scenarios relevant to smart-grid operation: DC load steps and DC-side voltage sags (fault ride-through, FRT). Time-domain simulations show that, for the tested operating point, the H∞-controlled synchronverter improves damping, reduces voltage deviations and limits current peaks compared with droop control. Frequency-domain analyses based on sensitivity functions confirm performance/robustness trade-offs for the considered disturbances. The results indicate that practical robust multivariable control can enhance synchronverter-driven LVDC microgrid resilience and FRT capability.*

Keywords: *LVDC microgrid; Synchronverter; Grid-forming inverter; H_∞ control; Fault ride-through.*

Date of Submission: 03-01-2026 Date of acceptance: 11-01-2026

I. INTRODUCTION

The ongoing transformation of electrical power systems towards large shares of converter-interfaced renewable generation, storage and flexible loads is profoundly changing the way grid stability is achieved. Conventional synchronous machines are being progressively displaced by power electronic interfaces, which reduces the system's natural rotational inertia and makes frequency and voltage control more dependent on local control algorithms and communication infrastructures [01], [02], [03]. At the distribution level, networks are evolving into active smart grids hosting a high density of distributed energy resources (DERs), LVDC networks and prosumers [04], [05], [06].

In this context, grid-forming inverters and virtual synchronous machine (VSM) concepts such as the synchronverter have emerged as key enablers of converter-dominated power systems. They emulate the dynamic behaviour of synchronous generators, including inertial response and primary frequency control, while interfacing renewable sources and storage units [07], [08], [09]. Zhong's framework of "power-electronics-enabled autonomous power systems" explicitly promotes this shift towards networks where local power electronics, rather than central dispatch, provide the primary layer of stability and power quality [09].

LVDC microgrids are increasingly investigated as a natural platform to integrate photovoltaics, storage, electric vehicles and DC loads with reduced conversion stages [10], [11], [12]. However, the dynamic coupling between a LVDC microgrid and the surrounding AC macro-grid through a grid-forming interface remains challenging, especially when fault ride-through (FRT), inertial support and robust performance under modelling uncertainties must be considered simultaneously [07], [13], [14].

Classical P–Q droop control is widely used in AC and DC microgrids for power sharing and voltage/frequency support, but it is sensitive to parameter uncertainties, grid strength and measurement noise [15], [16]. Robust and adaptive control methods, including H_∞ control, have therefore been investigated to improve disturbance rejection and guarantee stability under bounded model uncertainties [17], [18], [19], [20]. Yet, there is still relatively little work that combines:

1. a detailed small-signal model of a synchronverter interconnecting a LVDC microgrid with an AC macro-grid, including virtual inertia, droop behaviour and storage dynamics;
2. a systematic robust control synthesis (e.g. H_∞) explicitly formulated on that model; and
3. a quantitative comparison with a droop-based benchmark under scenarios directly relevant to

operation (FRT, load steps, active-power disturbances).

This paper addresses this gap by:

- deriving a small-signal state-space model of a LVDC microgrid whose DC bus is connected to an AC macro-grid through a synchronverter acting as a grid-forming interface;
- designing a multivariable robust H_∞ controller around this model, targeting DC bus voltage regulation, virtual inertia support and FRT capability in the presence of model uncertainties and disturbances;
- comparing its performance with a tuned droop-based PI controller under two scenarios: load steps ("droop test") and DC-side voltage sags (FRT).

The emphasis is not on pushing H_∞ control theory to its limits, but on demonstrating that such a robust controller can be practically embedded in a synchronverter-based LVDC microgrid and how it compares, on a realistic example, with a conventional droop controller.

II. PROBLEM STATEMENT AND ASSUMPTION

2.1 – Problem statement

The system under study is a low-voltage DC (LVDC) microgrid whose DC bus aggregates distributed generation, storage and DC loads, and is interfaced to the AC macro-grid through a grid-forming synchronverter. The synchronverter must :

1. regulate the DC bus voltage;
2. provide virtual inertia and damping to support frequency dynamics;
3. contribute to FRT capability under AC/DC-side disturbances.

The small-signal model is written as:

$$\begin{cases} \dot{x} = Ax + Bu + Ew \\ y = Cx + D_u u + D_w w \end{cases} \tag{1}$$

where:

- $x \in \mathbb{R}^n$ collects the internal states (inductor current i_L, DC bus voltage v_{bus}, source current i_{src}, battery state of charge SOC, virtual frequency deviation ω and active/reactive power dynamics P_{dyn}, Q_{dyn});
- u is the control input vector applied by the synchronverter;
- w groups disturbances (load current steps, input-voltage sags, uncertain active-power injections);
- y includes the measured variables used for feedback (at least v_{bus}, ω, i_L).

The goal is to design a multivariable controller $K(s)$ such that the closed-loop interconnection of $P(s)$ and $K(s)$ is internally stable and satisfies:

- acceptable time-domain performance (voltage and frequency regulation, current limitation, FRT) for the tested disturbances;
- robustness margins in the frequency domain (sensitivity and complementary sensitivity norms);
- improved performance compared to a classical droop-based PI controller.

In the H_∞ framework, we introduce performance, control and uncertainty weights:

$$z = \begin{bmatrix} W_p e \\ W_u u \\ W_w w \end{bmatrix}, \quad e = y_{ref} - y \tag{2}$$

and seek a stabilising controller $K(s)$ such that:

$$\|T_{zw}(s)\|_\infty < \gamma \tag{3}$$

for some $\gamma > 0$, where T_{zw} is the closed-loop transfer from disturbances w to weighted outputs z.

2.2 – Main Assumptions

To keep the model tractable while preserving the essential dynamics, the following assumptions are adopted:

- The LVDC microgrid is represented by a single DC bus aggregating converters and loads; individual converter dynamics are not detailed.
- The synchronverter is the unique interface with the AC macro-grid, which is approximated as a stiff voltage source at nominal frequency.
- The model is a continuous-time, averaged, small-signal model around a nominal operating point $(V_{bus,0}, P_0)$
- Virtual synchronous machine behaviour is captured by a swing-like equation:

$$J_v \dot{\omega} = -D_v \omega - m P_{dyn} + d_\omega \tag{4}$$

where J_v and D_v are virtual inertia and damping, m is the internal P–ω droop coefficient and P_{dyn} is the active-power state.

- Reactive-power dynamics are represented by Q_{dyn} with a coupling to the DC bus voltage through a parameter nnn, which acts as a Q–V stiffness coefficient.
- SOC dynamics are much slower than electrical transients but kept in the model for coherence with energy-storage representation.
- Communication delays are neglected at the small-signal level; in practice, the H_∞ controller would be discretised with a sufficiently high sampling frequency.
- Disturbances (load steps, power impulses, input-voltage sags) are bounded and chosen within realistically admissible ranges; extreme fault conditions leading to protection trips are not addressed.

III. MODELING AND CONTROL DESIGN

This section presents the modelling framework and control synthesis adopted in this work. First, a small-signal state-space model of the synchronverter-based LVDC microgrid is derived. Then, a reduced-order representation is introduced and used for robust H∞ controller synthesis. A classical droop-based controller is finally described as a benchmark.

3.1 – System Configuration

The system consists of a low-voltage DC microgrid interfaced with an AC network through a synchronverter-based voltage-source converter operated in grid-forming mode. The synchronverter and the DC network are modelled together as a single multivariable dynamical system. **Fig. 1** illustrates the physical architecture of the synchronverter-interfaced LVDC microgrid together with associated state variables used for small-signal modelling.

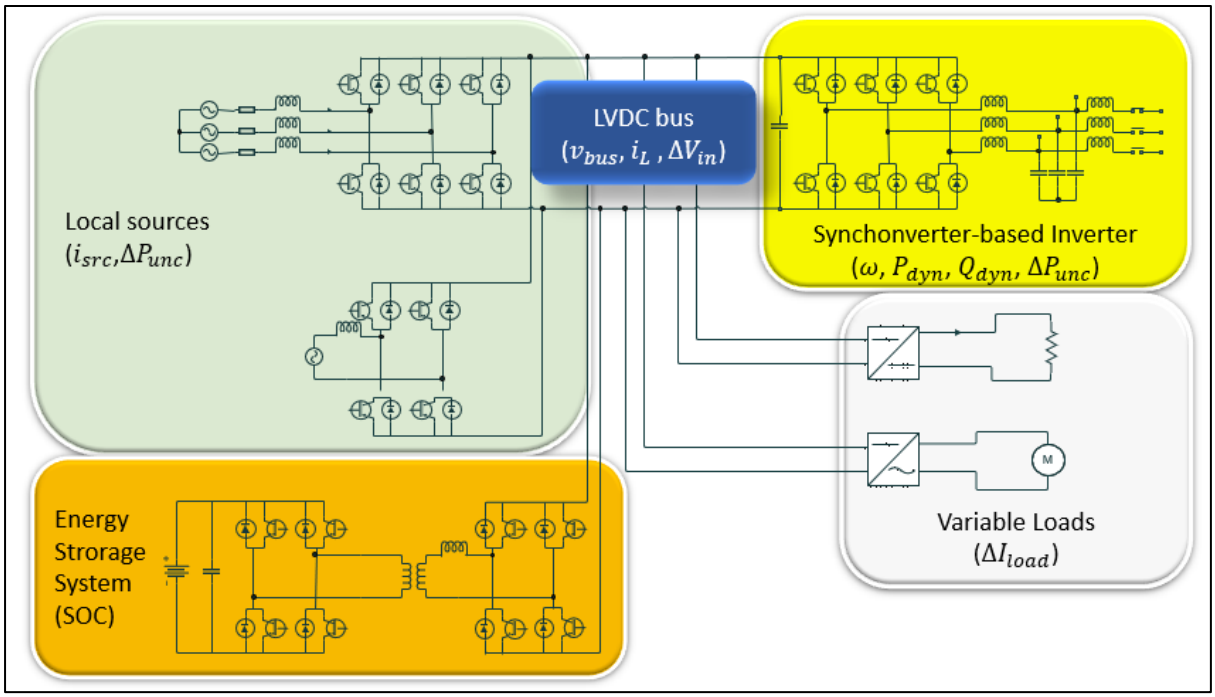

Fig. 1 Physical architecture and state variables of the synchronverter-interfaced LVDC microgrid

The synchronverter introduces virtual inertia and damping through internal power–frequency and power–voltage couplings, enabling frequency and voltage dynamics to be explicitly represented in the system model. Control actions are applied through the internal synchronverter control channels.

Two control structures are considered:

- a multivariable H_∞ controller designed on a reduced-order model,
- a conventional droop-based PI controller used for comparison.

3.2 – State-Space Representation of the LVDC Microgrid with Synchronverter

A seven-state small-signal model is derived. The state vector is:

$$x = [i_L \quad v_{bus} \quad i_{src} \quad SOC \quad \omega \quad P_{dyn} \quad Q_{dyn}]^T \tag{5}$$

The linearized system is written as:

$$\begin{cases} \dot{x} = Ax + Bu + Ew \\ y = Cx \end{cases} \tag{6}$$

where $y = [v_{bus} \quad \omega \quad i_L]^T$ is the output vector.
$u = [u_1 \quad u_2 \quad u_3]^T$ the control input vector corresponding to the synchronverter's internal control channels
$w = [\Delta I_{load} \quad \Delta V_{in} \quad \Delta P_{unc}]^T$ the disturbance vector

The matrix A embeds :

- the dynamics of the DC filter defined by line resistance R, inductance L and the DC-bus capacitance C_{dc};
- the virtual inertia J_v and damping D_v in the swing-like dynamics of ω;
- the internal droop couplings m (P–ω) and n (Q–V);
- and the slow storage dynamics driven by the source current;

$$A = \begin{bmatrix} -\frac{R}{L} & -\frac{1}{L} & 0 & 0 & 0 & 0 & 0 \\ \frac{1}{C_{dc}} & 0 & -\frac{1}{C_{dc}} & 0 & 0 & 0 & 0 \\ 0 & 0 & -\alpha_{src} & 0 & 0 & 0 & 0 \\ 0 & 0 & -\frac{1}{C_{batt}} & 0 & 0 & 0 & 0 \\ 0 & 0 & 0 & 0 & -\frac{D_v}{J_v} & -\frac{m}{J_v} & 0 \\ 0 & k_{Pv} & 0 & 0 & 0 & -\frac{1}{\tau_P} & 0 \\ 0 & -\frac{n}{\tau_Q} & 0 & 0 & 0 & 0 & -\frac{1}{\tau_Q} \end{bmatrix} \tag{7}$$

The control input matrix B, disturbance matrix E and output matrix C are given by:

$$B = \begin{bmatrix} 0 & 0 & 0 \\ 0 & 0 & 0 \\ \frac{1}{\tau_s} & 0 & 0 \\ 0 & 0 & 0 \\ 0 & \frac{1}{J_v} & 0 \\ 0 & 0 & \frac{1}{\tau_P} \\ 0 & 0 & 0 \end{bmatrix}; \qquad E = \begin{bmatrix} 0 & \frac{1}{L} & 0 \\ -\frac{1}{C_{dc}} & 0 & 0 \\ 0 & 1 & 0 \\ 0 & 0 & 0 \\ 0 & 0 & 0 \\ 0 & 0 & 1 \\ 0 & 0 & 1 \end{bmatrix}; \qquad C = \begin{bmatrix} 0 & 1 & 0 & 0 & 0 & 0 & 0 \\ 0 & 0 & 0 & 0 & 1 & 0 & 0 \\ 1 & 0 & 0 & 0 & 0 & 0 & 0 \end{bmatrix} \tag{8}$$

All numerical values of the model parameters appearing in matrices A , B and E are summarized in **Tab. 1** for reproducibility.

Tab. 1 – Model Parameters and Nominal Values

Symbol	*Description*	*Value*	*Unit*
C_{batt}	Battery capacity	*2500*	Ah
C_{dc}	DC bus capacitance	$100e^{-6}$	F
D_v	Virtual damping	*0.05*	$W.s.rad^{-1}$
f	Base frequency	*50*	Hz
J_v	Virtual inertia	*0.5*	$kg.m^2$
k_{Pv}	Vbus → P_dyn sensitivity	*0.01*	$W.V^{-1}$
L	Line inductance	$3e^{-3}$	H

$\boldsymbol{m}$	Active-power droop coefficient (P–ω)	*0.05*	$rad.s^{-1}.W^{-1}$
$\boldsymbol{n}$	Reactive-power droop / Q–V stiffness	*0.02*	$V.var^{-1}$
$\boldsymbol{R}$	Line resistance	*0.05*	Ω
$\boldsymbol{S_{base}}$	Power base	*20000*	VA
$\boldsymbol{V_{bus,base}}$	DC bus base voltage	*700*	V
$\boldsymbol{\alpha_{src}}$	Source current time-constant	*0.5*	s^{-1}.
$\boldsymbol{\tau_P}$	Time constant P_{dyn}	*0.1*	s
$\boldsymbol{\tau_Q}$	Time constant Q_{dyn}	*0.1*	s

3.3 – Model Reduction and H_∞ Control Synthesis

Controllability and observability analyses indicate that a reduced-order representation is sufficient for control synthesis. A reduced plant P_{red} is therefore obtained via a similarity transformation preserving the dominant modes.

An H_∞ controller is synthesised on P_{red} using standard weighting functions W_p, W_u and W_w. The resulting controller is implemented on the full-order model for time- and frequency-domain evaluation

3.4 – Benchmark Droop-Based Controller

A classical droop-based PI controller acting on DC bus voltage deviation is implemented for comparison purposes. Its tuning follows standard heuristic rules and does not involve explicit robustness optimisation.

IV. SIMULATION RESULTS AND DISCUSSION

Time-domain simulations and frequency-domain analyses are performed on the full-order LVDC microgrid model in order to evaluate voltage regulation, frequency dynamics, current behaviour and robustness of the proposed control strategy. The performance of the robust H_∞ controller is compared against both the open-loop system and a classical droop-based PI controller under identical disturbance scenarios.

The simulations are conducted in continuous time using linearised small-signal models. All variables are expressed as deviations around the nominal operating point.

4.1 – H_∞ Controller Characteristics

The H_∞ controller is obtained from the reduced-order plant using a standard weighted synthesis procedure. The synthesis converges with a closed-loop H_∞ performance level of $\gamma = 2.34185$, corresponding to the optimal value returned by the *hinfsyn* procedure in MATLAB.
The controller is implemented as a continuous-time dynamic compensator:

$$\begin{cases} \dot{x}_K = A_K x_K + B_K y \\ u = C_K x_K + D_K y \end{cases} \tag{9}$$

The controller order corresponds to the reduced plant order retained for synthesis and remains compatible with real-time implementation. In this study, the reduced plant has order $r = 5$, and therefore the resulting H_∞ controller also has order 5 with:

$$A_K = \begin{bmatrix} 3.17538 & -29.98859 & -0.01639 & 0.03278 & 0.00397 \\ 978.22124 & -655.76933 & -1.15863 & 2.31741 & -0.51484 \\ 0.02009 & 0.00667 & -9.99829 & 4.61118e-5 & -0.31818 \\ -0.04017 & -0.01335 & 4.61097e-5 & -10.00009 & 4.80816e-5 \\ 0.00017 & 0.00016 & 0.00114 & 3.88152e-7 & -0.21323 \end{bmatrix}$$

$$B_K = \begin{bmatrix} 0.62395 & 1.08151e-5 & 0.15898 \\ 6.44594 & -1.71983e-7 & 0.49838 \\ -0.00079 & 0.00920 & -0.00013 \\ 0.00158 & -3.78306e-9 & 0.00027 \\ -8.86494e-6 & 0.00605 & -1.38608e-6 \end{bmatrix}$$

$$C_K = \begin{bmatrix} 5.26071 & -13.05575 & -0.00658 & 0.01317 & -0.01266 \\ 28.16871 & -0.59547 & -.03270 & 0.06540 & -0.03244 \\ 2.72338e-5 & -6.80890e-7 & 6.57428e-5 & 6.32903e-8 & -0.91090 \end{bmatrix}$$

$$D_K = \begin{bmatrix} 0 & 0 & 0 \\ 0 & 0 & 0 \\ 0 & 0 & 0 \end{bmatrix}$$

4.2 – Closed-Loop Configuration

The closed-loop system is obtained by interconnecting the full-order LVDC microgrid model with either:

1. the synthesized H_∞ controller, or
2. a classical droop-based PI controller acting on the DC bus voltage deviation.

Both controllers use the same measurement signals, and the same disturbance inputs are applied in all simulations to guarantee a fair comparison. The synchronverter parameters are kept identical for all cases unless explicitly stated.

In the implementation, the H_∞ closed-loop model explicitly returns both the system outputs and the control inputs, whereas the droop-based PI controller is implemented in a single-output form.

Fig. 2 illustrates the generalized closed-loop interconnection used for H_∞ synthesis, highlighting the separation between the physical plant dynamics, the reduced-order control model and the weighted performance channels defining the transfer function T_{zw}.

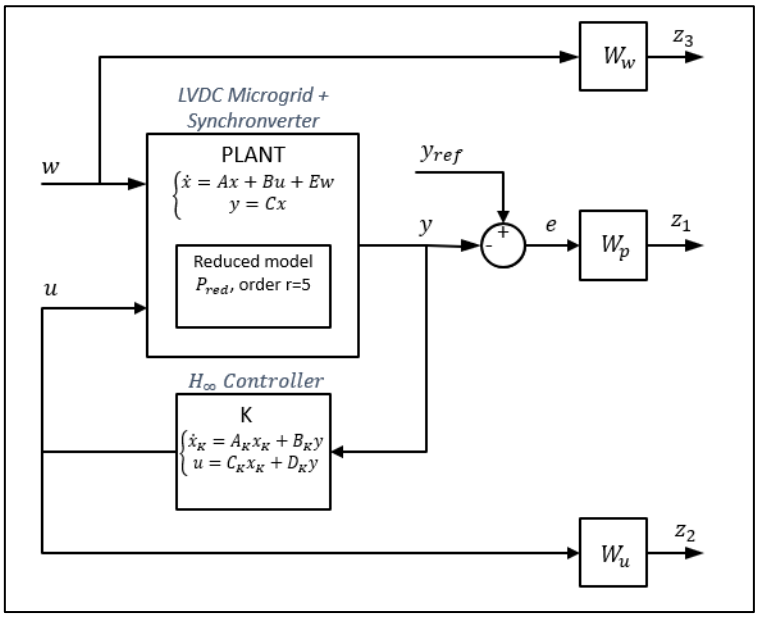

Fig. 2 Closed-loop generalized plant and H_∞ controller interconnection (T_{zw})

In **Fig. 2**, the reduced-order model P_{red} is used exclusively for controller synthesis, whereas all time- and frequency-domain simulations are carried out on the full-order plant.

4.3 – Load Step Response (Droop Test)

A load-step scenario is first considered to evaluate the DC bus voltage regulation capability and the associated frequency dynamics. At $t = 0.2\ s$, a step increase in the DC load current ΔI_{load} is applied to the microgrid. This disturbance emulates a sudden increase in local demand while the AC-side voltage remains nominal. The resulting time-domain responses are shown in **Fig. 3**.

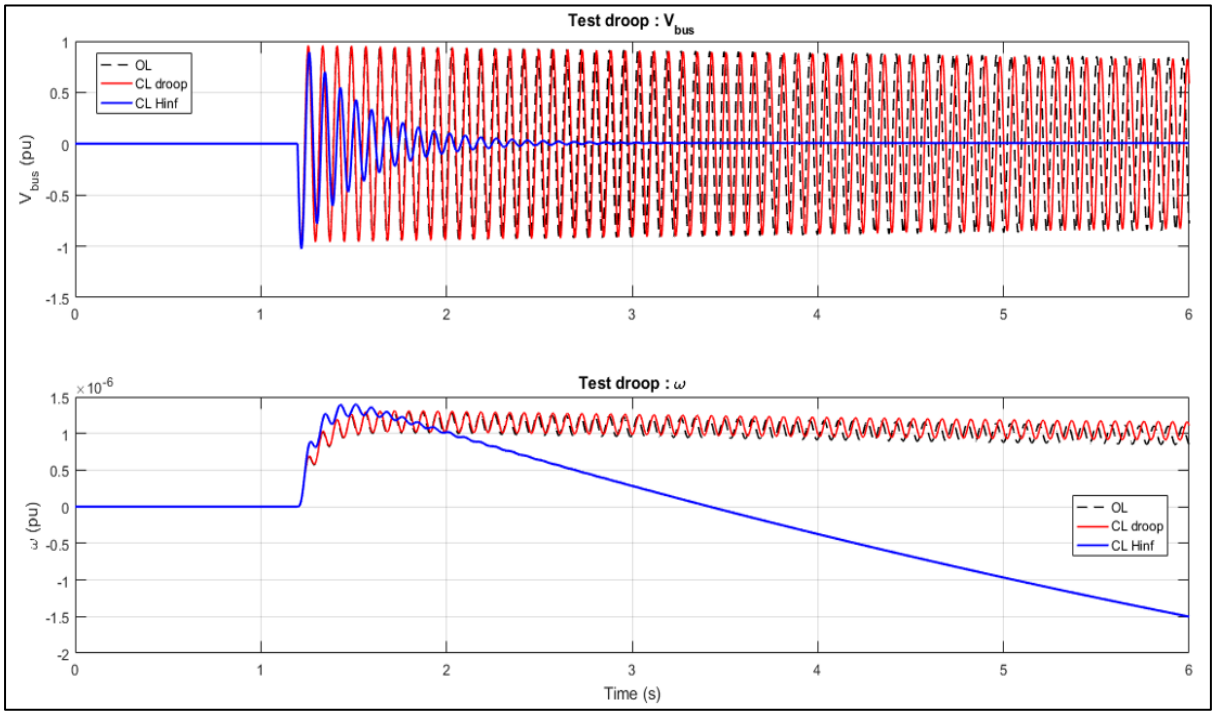

Fig. 3 Load-step response: open-loop, droop-based control and H_∞ control comparison

As shown in **Fig. 3**, the open loop DC-bus voltage v_{bus} exhibits a pronounced drop followed by oscillations, reflecting the limited damping of the physical plant and the interaction between the DC-link capacitance and the converter dynamics. The frequency deviation ω exhibits a small transient excursion and then settles to a value on the order of 10^{-6} pu. This residual offset is numerically negligible and reflects the very small active-power imbalance left after the disturbance. This behaviour reflects a near-perfect active-power equilibrium at steady state.

This figure also shows that the droop-based PI controller reduces the voltage deviation compared to open loop, but the response remains under-damped, with noticeable overshoot and a relatively long settling time. The frequency deviation is slightly improved during the transient but remains of the same negligible order of magnitude at steady state. In other words, the droop controller provides basic voltage support while leaving a modest oscillatory behaviour on v_{bus}, and the impact on the steady-state frequency deviation remains practically imperceptible in this test.

By contrast, the H_∞ controller achieves a significantly improved transient behaviour, as clearly visible in **Fig. 3**. The DC-bus voltage drop is smaller, oscillations are strongly attenuated, and the voltage recovers faster toward its nominal value, with very limited overshoot. The frequency deviation exhibits a reduced peak and a smoother transient, and it quickly returns to values numerically indistinguishable from zero in per-unit. This confirms that the H_∞ controller enhances damping and disturbance rejection while preserving the nominal frequency in steady state for the considered load-step scenario.

Overall, the load-step test shows that the H_∞-controlled system outperforms classical droop control in terms of DC-bus voltage regulation and transient behaviour, while maintaining a negligible steady-state frequency deviation.

4.4 – Fault Ride-Through (FRT) performance

The Fault Ride-Through capability of the LVDC microgrid is evaluated by introducing a temporary input-voltage sag ΔV_{in}. The voltage sag is applied between $t_1 = 1.5\,s$ and $t_2 = 3.6\,s$. The corresponding FRT responses are reported in **Fig. 4**.

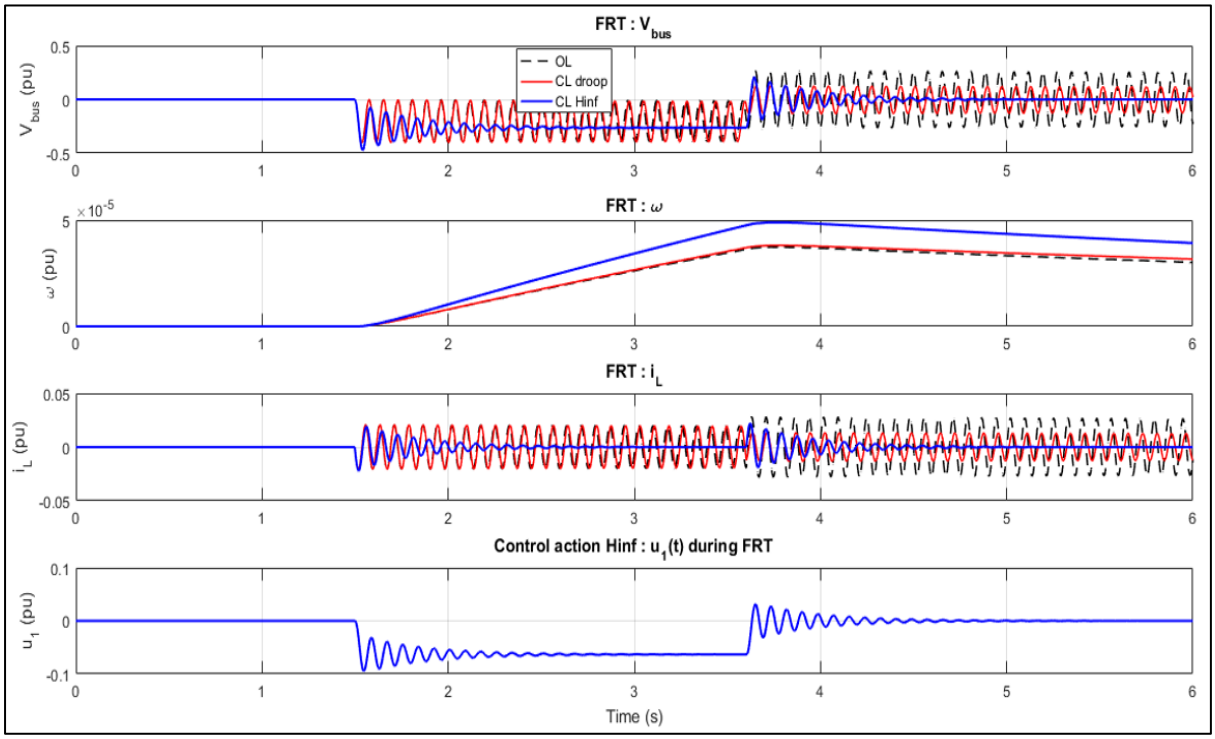

Fig. 4 Fault Ride-Through (FRT) response under DC-side voltage sag

In open loop (**Fig. 4**), the imposed voltage sag propagates almost directly to the DC bus. The DC-bus voltage v_{bus} exhibits a pronounced drop during the interval $[t_1, t_2]$ followed by oscillatory behaviour after fault clearance. The inductor current i_L undergoes amplified oscillations with elevated peak values, while the frequency deviation ω is significantly disturbed, reflecting the lack of active damping and disturbance rejection.

With the droop-based controller (**Fig. 4**), the voltage sag dept his reduced but oscillations persist both during the sag interval and after recovery. The inductor current still exhibits relatively large transient peaks, and the frequency deviation remains weakly damped, indicating limited capability to cope with fast voltage disturbances.

When the H_∞ controller is applied, **Fig. 4** shows that the controller maintains bounded voltage deviations during the sag and ensures a smooth post-fault recover. The inductor current peaks are clearly reduced compared to both the open-loop and droop-controlled cases. The frequency deviation ω remains small throughout the disturbance and does not exhibit sustained oscillations.

This comparison shows that the H_∞ controller effectively reshapes the closed-loop dynamics during voltage sag conditions, providing improved damping and disturbance rejection under FRT scenarios.

4.5 – Frequency-domain Robustness Analysis

The robustness characteristics of the closed-loop system are assessed through three standard frequency-domain indicators:
(i) the loop transfer function $L = P_{control}K$,
(ii) the sensitivity function S, and
(iii) the complementary sensitivity function T.
These quantities are routinely used in robust control to evaluate disturbance rejection, noise attenuation and stability margins. Frequency-domain robustness properties are further analysed using singular value plots of the loop transfer function and the associated sensitivity functions. The singular value of the functions $L(j\omega)$, $S(j\omega)$ and $T(j\omega)$ are respectively plotted in **Fig. 5**, **Fig. 6** and **Fig. 7**.

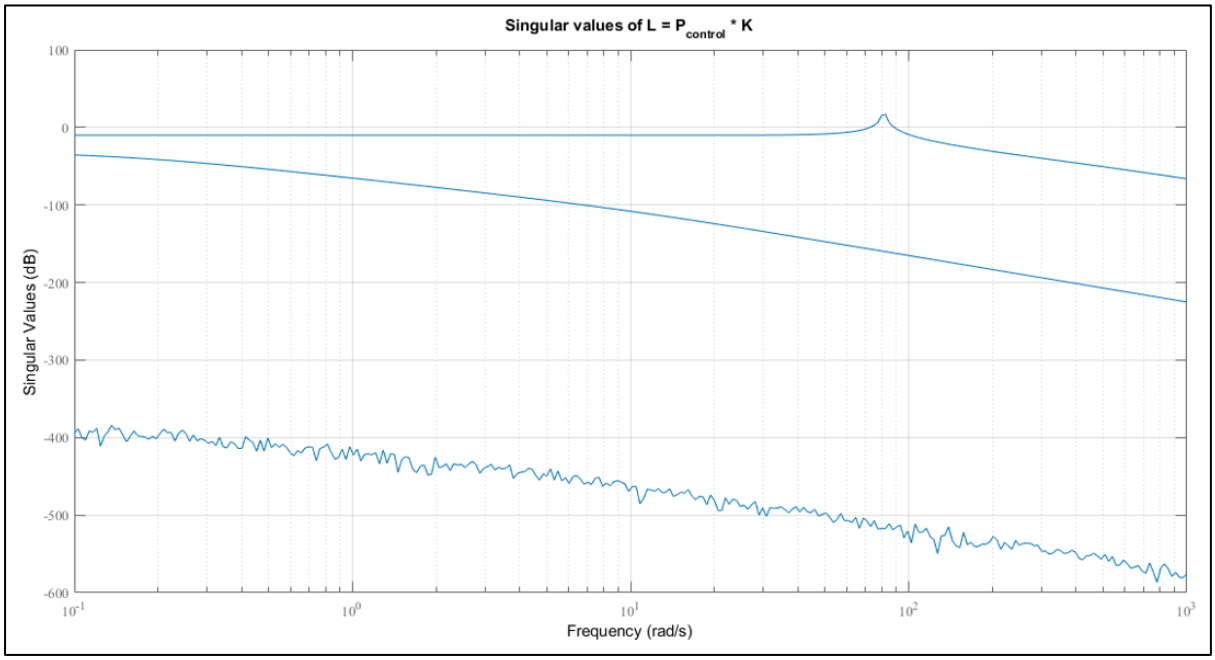

Fig. 5 Singular value plot of the loop transfer function $L(j\omega)$

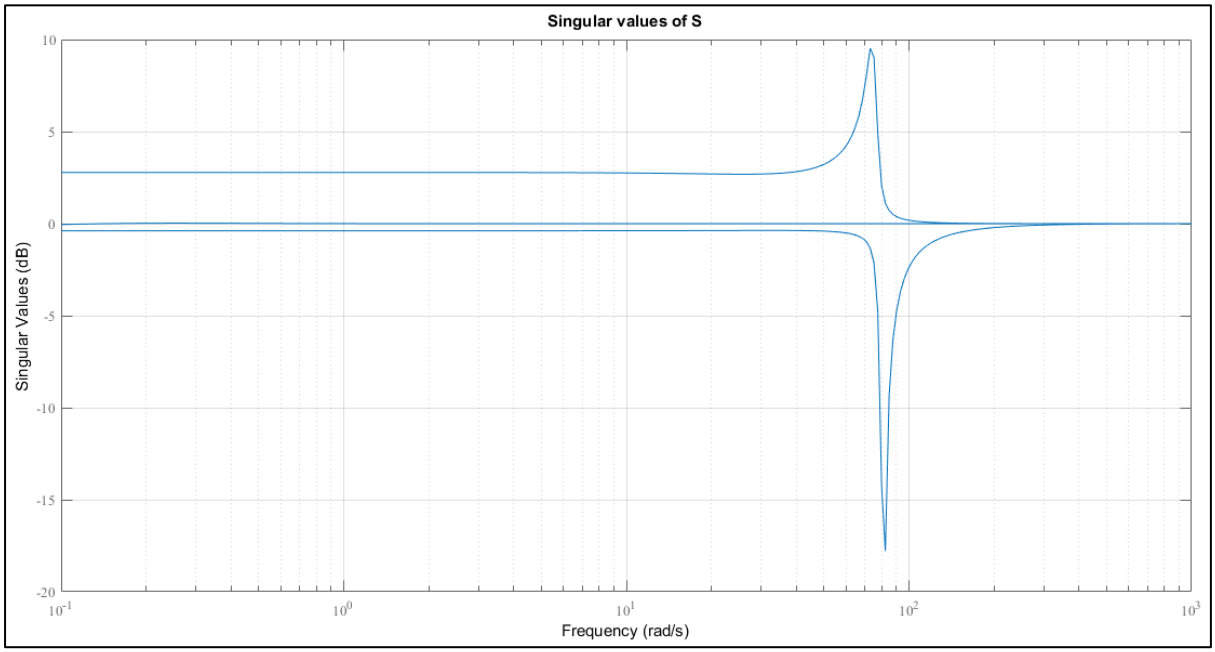

Fig. 6 Singular value plot of the sensitivity function $S(j\omega)$

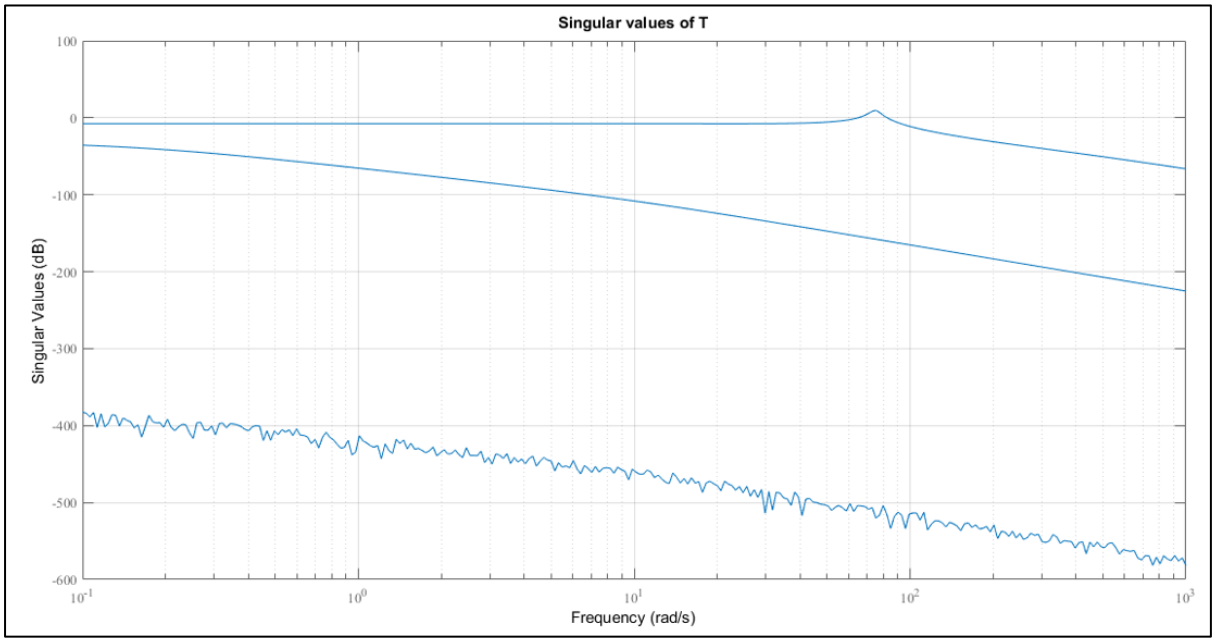

Fig. 7 Singular value plot of the complementary sensitivity function $T(j\omega)$

As illustrated in **Fig. 5**, The loop-transfer singular values $\sigma(L(j\omega))$ show sufficiently high gain at low frequencies, demonstrating that the H_∞ controller provides strong low-frequency authority for DC-bus voltage regulation. The gain roll-off occurs smoothly as frequency increases, with no excessive amplification near crossover, indicating the absence of lightly damped hidden modes and providing comfortable robustness margins. This behaviour is consistent with the well-damped time responses observed in the droop and FRT scenarios.

The sensitivity function $S = (I + L)^{-1}$ characterises disturbance rejection at low frequencies. **Fig. 6** confirms that the sensitivity function remains below 0 dB over the dominant bandwidth of the microgrid dynamics, confirming effective attenuation of low-frequency disturbances such as load steps and voltage sags. The peak value $\|S\|_\infty$ remains moderate, well aligned with the target H_∞ performance level γ.

The complementary sensitivity function $T = I - S$ captures the amplification of high-frequency noise and unmodelled dynamics. The high-frequency roll-off observed in **Fig. 7** indicates effective attenuation of measurement noise and unmodelled fast dynamics, which prevents excitation of switching harmonics or neglected fast converter modes. The moderate peak value $\|T\|_\infty$ confirms that the high-frequency dynamics remain well controlled.

Overall, the trends of L, S and T jointly validate the robustness of the proposed H_∞ controller, showing adequate stability margins and disturbance/noise shaping compatible with the operational requirements of LVDC microgrids.

The computed robustness metrics are $\|S\|_\infty = 3.091$ and $\|T\|_\infty = 3.075$. While these values confirm that the designed controller attains the H_∞ performance level returned by synthesis ($\gamma = 2.34185$), they also indicate a moderate robustness margin: $\|S\|_\infty$ and $\|T\|_\infty$ greater than unity reflect a non-negligible worst-case amplification of certain disturbances and model uncertainties. This observation highlights the standard H_∞ trade-off: the present weighting choice privileges time-domain disturbance rejection and reduced transients at the expense of tighter worst-case norms. A retuning of the weights W_p, W_u, W_w (or gain-scheduling) could be adopted in future work to reduce $\|S\|_\infty$ if stricter worst-case guarantees are required.

4.6 – Discussion

The simulation results highlight the differences between open-loop behaviour, classical droop control and the proposed H_∞ controller when applied to a synchronverter-based LVDC microgrid. Several observations can be drawn from the presented scenarios.

First, the open-loop system exhibits lightly damped dynamics dominated by the interaction between the DC-link capacitance, the inductor current and the synchronverter electromechanical emulation. Both the load-step and FRT tests reveal significant sensitivity to disturbances, with large oscillations and slow recovery. This confirms that, in its nominal configuration, the synchronverter requires active control to achieve acceptable performance under realistic operating conditions.

Second, the droop-based PI controller provides only partial improvement. While the bus-voltage deviation is reduced compared to open loop, the inherent under-damped behaviour of the system remains visible. Oscillations persist during both the load-step and FRT events, and the converter's ability to reject disturbances remains limited. This behaviour is consistent with known limitations of droop control in converter-dominated microgrids, where static gains alone are insufficient to ensure dynamic performance or robust damping.

Third, the H_∞ controller significantly improves the transient response in all tested scenarios. Its main benefits include:

- enhanced damping of the DC-bus voltage dynamics,
- reduced inductor-current peaks,
- minimal deviation of the virtual frequency,
- fast and smooth post-fault recovery.

These improvements stem from the controller's ability to shape the multivariable dynamics of the synchronverter, particularly through coordinated action on the voltage, current and frequency channels. Unlike droop control, which provides limited dynamic influence, the H_∞ controller offers frequency-selective disturbance rejection and robustness against unmodelled dynamics.

The frequency-domain analysis supports these conclusions. The sensitivity and complementary sensitivity functions remain within acceptable bounds, confirming satisfactory stability margins and noise shaping. The loop-transfer behaviour indicates appropriate low-frequency authority as well as a controlled high-frequency roll-off, preventing interaction with parasitic converter dynamics.

Finally, the negligible steady-state frequency deviation (on the order of 10^{-6} pu) observed in all closed-loop cases indicates that the synchronverter maintains an almost perfect power balance after disturbances. This is consistent with the synchronverter behaving as the grid-forming reference in a DC microgrid, where primary frequency support does not require droop-induced steady-state offsets.

Overall, the results demonstrate that robust multivariable control can substantially enhance the operational behaviour of synchronverter-operated LVDC microgrids, particularly under fast or severe disturbances. Compared with classical droop control, the H_∞ approach provides superior damping, improved disturbance rejection and enhanced FRT capability, without introducing excessive control effort or compromising stability.

V. CONCLUSION

This work has presented the modelling, robust control design and performance assessment of a synchronverter-based LVDC microgrid operated in grid-forming mode. A seven-state small-signal model was derived, explicitly incorporating DC-link dynamics, source-current behaviour, virtual inertia, damping, and internal active and reactive power states. A reduced-order representation was constructed to enable well-conditioned H_∞ synthesis, from which a multivariable robust controller was obtained.

Time-domain simulations demonstrated that the proposed H_∞ controller substantially improves voltage regulation, damping and disturbance rejection compared with both the open-loop system and a classical droop-based PI controller. In the droop test, the H_∞ controller reduced voltage deviations and eliminated oscillations while maintaining negligible steady-state frequency error. Under FRT conditions, the controller ensured bounded voltage deviations, reduced current peaks and smooth post-fault recovery, outperforming the droop controller in all respects.

Frequency-domain analyses confirm that the closed-loop system meets the designed H_∞ performance level. The loop-transfer function provides sufficient low-frequency authority, while the sensitivity and complementary sensitivity remain within the bounds set by the chosen weighting functions. The reported $\|S\|_\infty$ and $\|T\|_\infty$ values reflect the design trade-offs and should be used to guide follow-up tuning for stricter worst-case robustness if required.

Overall, the results show that robust multivariable control can significantly enhance the dynamic performance and resilience of synchronverter-driven LVDC microgrids, particularly in disturbance-rich environments. The proposed approach offers a promising pathway toward stabilising converter-dominated distribution networks and supporting advanced functionalities such as virtual inertia, coordinated voltage regulation and fault ride-through.

Future extensions will focus on integrating nonlinear and large-signal effects, addressing converter saturation and protection limits, and validating the proposed control strategy on real-time or hardware-in-the-loop experimental platforms.

REFRENCES

[01]. Hadjsaid, N. and Sabonnadière, J.-C. [2009] "Power Systems and Restructuring" ISTE Ltd and John Wiley & Sons, Inc.

[02]. Buchholz, B.M. and Styczynski, Z. [2014] "Smart Grid – Fundamentals and Technologies in Electricity Networks" Springer-Verlag Berlin Heidelberg.

[03]. Salman, S.K. [2017] "Introduction to the Smart Grid – Concepts, Technologies and Evolution" The Institution of Engineering and Technology.

[04]. CIRED Working Group on Smart Grids [2013] "Smart Grids on the Distribution Level – Hype or Vision ?" CIRED Report.

[05]. Kabalci, E. [2019] "Technical Challenges and Enhancements in Smart Grid Applications" Smart Grids and Their Communication Systems, Springer Nature Singapore Pte Ltd: pp. 81–119.

[06]. Lai, C.S., Lai, L.L. and Lai, Q.H. [2021] "Smart Grids and Big Data Analytics for Smart Cities" Springer Nature Switzerland AG.

[07]. Lin, Y., Eto, J.H., Johnson, B.B., Flicker, J.D., Lasseter, R.H., Villegas Pico, H.N., Seo, G.S., Pierre, B.J. and Ellis, A. [2020] "Research Roadmap on Grid-Forming Inverter" National Renewable Energy Laboratory.

[08]. Lin, Y., Johnson, B., Dolphe, S. et al. [2021] "Final Technical Report: Stabilizing the Power System in 2035 and Beyond – Evolving from Grid-Following to Grid-Forming Distributed Inverter Controllers" National Renewable Energy Laboratory.

[09]. Zhong, Q.-C. [2020] "Power Electronics-Enabled Autonomous Power Systems – Next Generation Smart Grids" John Wiley & Sons Ltd.

[10]. Saravanan, S., Prabaharan, N. and Ramesh-Babu, N. [2019] "DC-DC Converters for Renewable Energy Applications" Smart Grid Systems – Modeling and Control, Apple Academic Press, Inc: pp. 107–128.

[11]. Prasanth Ram, J. and Rajasekar, N. [2019] "Design of PV System with Battery Storage" Smart Grid Systems – Modeling and Control, Apple Academic Press, Inc: pp. 12–40.

[12]. Mohanty, P., Sharma, K.R., Gujar, M., Kolhe, M. and Azmi, A.N. [2016] "PV System Design for Off-Grid Applications" Solar Photovoltaic System Applications – A Guidebook for Off-Grid Electrification, Springer International Publishing Switzerland.

[13]. Vasudevan, K.R., Ramachandaramurthy, V.K., Babu, T.S. and Pouryekta, A. [2020] "Synchronverter: A Comprehensive Review of Modifications, Stability Assessment, Applications and Future Perspectives" IEEE Access, Vol. 8.

[14]. Ayamolowo, O.J., Manditereza, P. and Kusakana, K. [2022] "An Overview of Inertia Requirement in Modern Renewable Energy Sourced Grid: Challenges and Way Forward" Journal of Electrical Systems and Information Technology.

[15]. Tiwari, R., Kumar, K. and Ramesh-Babu, N. [2019] "Control Strategies for Renewable Energy System" Smart Grid Systems – Modeling and Control, Apple Academic Press, Inc: pp. 65–106.

[16]. Mahmoud, M.S. and Al-Sunni, F.M. [2015] "Control and Optimization of Distributed Generation Systems" Springer International Publishing Switzerland.

[17]. Hossain, J. and Pota, H.R. [2014] "Robust Control for Grid Voltage Stability: High Penetration of Renewable Energy" Springer Science+Business Media Singapore.

[18]. Banerjee, A., Chaudhuri, N.R. and Kavasseri, R. [2018] "A Novel Explicit Disturbance Model-Based Robust Damping of Inter-Area Oscillations through MTDC Grids Embedded in AC Systems" IEEE.

[19]. Rezaei, M.M., Shojaeian, S. and Rouhollahi, R. [2020] "Robust Control of a Multi-Bus DC Microgrid Based on Adaptive Lyapunov Function Method" Journal of Electrical Systems and Information Technology.

[20]. Shafiee-Rad, M., Sadabadi, M.S., Shafiee, Q. and Jahed-Motlagh, M.R. [2020] "Robust Decentralized Voltage Control for Uncertain DC Microgrids" International Journal of Electrical Power & Energy Systems